14th Congress of the International Society for Photogrammetry

Hamburg 1980

Commission No. V
Working Group No. 3

Invited Paper

STATE-OF-THE-ART IN HOLOGRAMMETRY AND RELATED FIELDS

by

Ryszard J. Pryputniewicz
Department of Mechanical Engineering
Worcester Polytechnic Institute
Worcester, Massachusetts 01609
U. S. A.

ABSTRACT

Hologrammetry and speckle metrology have become very active areas of research, in recent years, and, as a result of this, there now exists quite a collection of techniques that are applicable to a wide variety of problems encountered in today's science and technology. This review presents state-of-the-art advances in these measuring techniques and demonstrates their utility in such applications as displacement and strain measurement, vibration analysis, studies of rotating structures, surface roughness measurement, nondestructive testing, contouring, as well as in biostereometrics.

Introduction

In the last decade, hologrammetry and its companion field of speckle metrology have grown tremendously and found numerous applications in such diverse fields as aerospace, automotive, electronics, machinery, transportation, equipment, packaging, and other industries, and even in medical and dental laboratories [1, 2]. All of these advances are well documented in various publications, too numerous to be even listed in this paper. And the field is still growing. Constantly, there are new ways found to apply hologrammetry and speckle metrology to solve problems that were unsolvable heretofore, as was excellently summarized by Erf [3, 4], Stetson [5], and Vest [6]. As new methematical procedures for quantitative interpretation of holograms and specklegrams are developed, it becomes easier to use these state-of-the-art techniques in various metrologic applications [7].

Interpretation of holographic images, however, is based on ones ability to delineate various parameters such as, for example, displacement, illumination and observation propagation directions, object surface normals, normals to fringes, etc. Recent studies [2, 8-10] show that pertinent relationships between the involved holographic parameters, because of their vectorial nature, can best be described by projection matrices; the projection matrix transforms a vector into its shadow on a surface. These new formulations allow a straightforward interpretation of holograms with the aid of programmable hand calculators, thus, reducing ones reliance on large digital computers for solution of governing equations. Furthermore, the relationships of hologram interferometry apply equally well to problems encountered in speckle metrology [2].

In the following, these and other most recent developments in hologrammetry and related fields will be presented and their utility in such applications as displacement and strain measurement, surface roughness measurement, contouring, and other areas, will be discussed.

Displacement measurement

The problem of extracting displacements directly from the fringes of hologram interferometry has been solved in a number of ways [11]. Most of these techniques require multiple observations of the holographically reconstructed image in order to reduce experimental errors. In these cases, one solves for the three components of the displacement vector that yield the least-square-error in an attempt to satisfy the overdetermined set of equations that is generated from the excess data as, for example, discussed in Reference 12. The above analysis require use of digital computers. The pertinent equations, however, can be reformulated in terms of projection matrices and solved on a programmable hand calculator, as discussed below.

It is well known that fringe localization, observed with orthogonal slit apertures, can be used to determine two components of object displacement transverse to the observation direction. The vector sum of these two components may be referred to as the observed object displacement $\underline{\underline{L}}_{ob}$. If we make two independent observations of the holographic image along directions $\hat{K}_2^1$ and $\hat{K}_2^2$, see Fig. 1, then the corresponding observed displacements $\underline{\underline{L}}_{ob}^1$ and $\underline{\underline{L}}_{ob}^2$ can be related to the total displacement vector $\underline{\underline{L}}$ by projection matrices $\underset{\sim}{P}^1$ and $\underset{\sim}{P}^2$, respectively, that is,

$$\underset{\sim}{L}^{1}_{ob} = \underset{\sim}{P}^{1}\,\underset{\sim}{L} \qquad (1)$$

and

$$\underset{\sim}{L}^{2}_{ob} = \underset{\sim}{P}^{2}\underset{\sim}{L}\ , \qquad (2)$$

where the projection matrices were defined as

$$\underset{\sim}{P}^{m} = -\hat{\underset{\sim}{K}}^{m}_{2}\,\hat{\underset{\sim}{K}}^{m}_{2} = \underset{\sim}{I} - \hat{K}^{m}_{2} \otimes \hat{K}^{m}_{2}\ , \quad m=1,2\ . \qquad (3)$$

In Eq. 3, $\hat{\underset{\sim}{K}}^{m}_{2}$ indicates a 3×3 antisymmetric matrix of the unit observation vector $\underset{\sim}{K}^{m}_{2}$, $\underset{\sim}{I}$ is a 3×3 identity matrix, and $\otimes$ denotes a matric product of $\hat{K}^{m}_{2}$ with itself (the operation $\hat{K}^{m}_{2} \otimes \hat{K}^{m}_{2}$ yields a matrix whose elements are all nine possible products of the three components of $\hat{K}^{m}_{2}$).

Neither Eq. 1 nor Eq. 2, by itself, can be inverted to yield $\underline{\underline{L}}$ because of the singularity of the projection matrices. Equations 1 and 2 may be combined, however, to yield an overdetermined set of equations

$$\begin{bmatrix} \underset{\sim}{L}^{1}_{ob} \\ \underset{\sim}{L}^{2}_{ob} \end{bmatrix} = \begin{bmatrix} \underset{\sim}{P}^{1} \\ \underset{\sim}{P}^{2} \end{bmatrix} \underset{\sim}{L}\ , \qquad (4)$$

which can be solved [2, 9] to yield

$$\underset{\sim}{L} = \left[\underset{\sim}{P}^{1} + \underset{\sim}{P}^{2}\right]^{-1}\left(\underset{\sim}{L}^{1}_{ob} + \underset{\sim}{L}^{2}_{ob}\right)\ . \qquad (5)$$

Equation 5 yields a value for $\underline{\underline{L}}$ whose two projections onto planes normal to $\hat{K}^{1}_{2}$ and $\hat{K}^{2}_{2}$ have the least-square-error with respect to $\underline{\underline{L}}^{1}_{ob}$ and $\underline{\underline{L}}^{2}_{ob}$. The above process may be extended to any number of observations by

$$\underset{\sim}{L} = \left[\sum_{m=1}^{r} \underset{\sim}{P}^{m}\right]^{-1}\left(\sum_{m=1}^{r} \underset{\sim}{L}^{m}_{ob}\right)\ , \qquad (6)$$

where r indicates total number of views. Equation 6 allows a straightforward, systematic solution for $\underline{\underline{L}}$ on a programmable hand calculator.

We should note, at this time, that Eq. 6 applies not only to the cases when fringe parallax is used in analysis of a holographic image, but also to cases which require simultaneous interpretation of two or more independent holograms of the same object (Fig. 2) and, therefore, when it is impossible to make continuous observations of the image. This latter case arises when we want to improve the accuracy for determination of the component of object displacement in the viewing direction, especially if the hologram is not very large. Furthermore, Eq. 6 may also be used in speckle metrology [13] where the magnitude and direction of observed displacements relate directly to the frequency and orientation of halo fringes.

Strain measurement

The demand for greater optimization in the load resisting structures have created a need for better experimental techniques for accurate measurement of structural deformations. Hologrammetry and related techniques are particularly suited for this application because they allow rapid, full-surface inspection of a tested object which does not require any special preparation. As a result of this, there were many techniques developed for holographic analysis of structures. For example, Dändliker et al. [14] have

developed an optoelectronic fringe interpolation technique, whereas Dubas and Schumann [15] proposed a theory of fringe localization requiring a complex apparatus of coupled telescops. More recently, Stetson [16-18] presented a theory, that permits a straightforward determination of homogeneous strains of arbitrarily three-dimensional objects; in the case of heterogeneous strains - average values are obtained. We call this technique the fringe vector method of holographic strain analysis, because it recognizes that any combination of homogeneous strain, shear, and rotation of an object yields fringes on its surface which can be described by a single vector. In the following, we shall briefly describe this new method and outline its use in strain analysis.

If an object undergoes a homogeneous deformation and/or rotation during the recording of a hologram, then, in the reconstruction, the object will be seen covered by a pattern of fringes that would appear to be generated along the lines of intersection of the object's surface with a set of parallel, equally spaced planes (Fig. 3), called fringe-locus planes. The fringe-locus planes are uniquely defined by the fringe vector whose magnitude is inversely proportional to the spacing between these planes and whose direction is normal to them. As such, the fringe vector $\underline{\underline{K}}_f$ can be expressed in terms of the matrix $\underset{\sim}{f}$ of strains, shears, and rotations of the object, and the first-order variations of the sensitivity vector $\underset{\sim}{g}$ as [17]

$$\underline{\underline{K}}_f = \underline{\underline{K}}\,\underset{\sim}{f} + \underline{\underline{L}}\,\underset{\sim}{g} \quad , \tag{7}$$

where $\underline{\underline{K}}$ is the sensitivity vector defined as the difference between the observation and illumination vectors (that is, $\underline{\underline{K}} = \underline{\underline{K}}_2 - \underline{\underline{K}}_1$) [19, 20], $\underline{\underline{L}}$ is the displacement vector, and $\underset{\sim}{g}$ is defined as

$$\underset{\sim}{g} = \frac{k}{R_o}\underset{\sim}{P}_2 - \frac{k}{R_i}\underset{\sim}{P}_1 \, . \tag{8}$$

In Eq. 8 R_i and R_o are radii of curvature of illumination and observation perspectives, respectively, while $\underset{\sim}{P}_1$ and $\underset{\sim}{P}_2$ represent corresponding projection matrices (see Eq. 3). What we are interested in is the matrix $\underset{\sim}{f}$ which can be decomposed into a matrix of strains and shears, $\underset{\sim}{e}$, and a matrix of rotations, $\underset{\sim}{\theta}$.

In order to solve Eq. 7 for the transformation matrix $\underset{\sim}{f}$ we perform multiple observations of the holographically reconstructed image. For each observation we determine the sensitivity vector $\underline{\underline{K}}$ and, also, we find the fringe vector $\underline{\underline{K}}_f$ that best fits the data from the entire region examined. We also use multiple views to obtain displacement $\underline{\underline{L}}$ of a point of interest on the object. For each view, we compute matrix $\underset{\sim}{g}$ and multiply it by $\underline{\underline{L}}$ to obtain perspective corrections to $\underline{\underline{K}}_f$. From multiple views, we obtain a set of equations of the type of Eq. 7, with the matrix $\underset{\sim}{f}$ common to all, which may be solved [18] to obtain

$$\underset{\sim}{f} = \left[\underline{\underline{K}}^T\underline{\underline{K}}\right]^{-1}\left[\underline{\underline{K}}^T\underline{\underline{K}}_{fc}\right] \quad , \tag{9}$$

where $\underline{\underline{K}}_{fc} = \underline{\underline{K}}_f - \underline{\underline{L}}\,\underset{\sim}{g}$ is the matrix formed by the fringe vectors corrected for perspective. Decomposition of the matrix $\underset{\sim}{f}$, computed from Eq. 9, into the symmetric part $\underset{\sim}{e}$ and the antisymmetric part $\underset{\sim}{\theta}$, that is,

$$\underset{\sim}{e} = \tfrac{1}{2}\left[\underset{\sim}{f} + \underset{\sim}{f}^T\right] \quad , \qquad \underset{\sim}{\theta} = \tfrac{1}{2}\left[\underset{\sim}{f} - \underset{\sim}{f}^T\right] \quad , \tag{10}$$

gives strains and shears, and rotations, respectively.

When the object deformations are not homogeneous over the entire body under study, they may, nonetheless, be approximately so over small regions of its

surface and projection matrices are very helpful in formulating the solution to this problem. It can be shown that, in this case, the surface strain-rotation matrix $\underset{\sim}{f}_s$ is

$$\underset{\sim}{f}_s = \underset{\sim}{f}\,\underset{\sim}{P}_n \quad , \tag{11}$$

where $\underset{\sim}{P}_n$ is the projection matrix defined as $\underset{\sim}{P}_n = \underset{\sim}{I} - \hat{n} \otimes \hat{n}$, with $\hat{n}$ being surface normal. It should be noted that the derivatives of observed displacement are not generally equal to surface strains and rotations of an object. They, become approximately equal to the extent that the viewing direction can be made parallel to the surface normal [21]. This condition is impossible to achive on any surface that exhibits three-dimensional contours, and it is difficult to achive even on a flat surface because of the spherical perspective of most viewing systems. However, the derivatives of observed displacement from two or more viewing directions can be used to extract surface strains and rotations [21].

Contouring

Many engineering problems require preparation of topographical maps of studied objects and hologrammetric techniques can be used to produce desired contours. This can be demostrated in an elegant way, using the definition of the fringe vector, when we recognize that the projection matrices of Eq. 8 operate on object displacement $\underline{\underline{L}}$ via Eq. 7.

Let us assume that the object is illuminated and observed with a spherical perspective and that both, the illumination and observation, radii are equal to each other (that is, $R_o = R_i = R$). Let us also assume that the strains and rotations are zero, that is, $\underset{\sim}{f} = 0$. Then, combining Eqs 7 and 8 we obtain

$$\mathbf{K}_f = \frac{k}{R}(\mathbf{L}_{ob} - \mathbf{L}_{ill}) \quad , \tag{12}$$

where $\underline{\underline{L}}_{ill}$ and $\underline{\underline{L}}_{ob}$ represent the observed displacements lateral to the illumination and observation directions, respectively, which are defined as

$$\mathbf{L}_{ill} = \mathbf{L}\left[\underset{\sim}{I} - \hat{K}_1 \otimes \hat{K}_1\right] \tag{13}$$

and

$$\mathbf{L}_{ob} = \mathbf{L}\left[\underset{\sim}{I} - \hat{K}_2 \otimes \hat{K}_2\right] \quad . \tag{14}$$

Finally, substitution of Eqs 13 and 14 into Eq. 12 and subsequent simplification yield

$$\mathbf{K}_f = \frac{k}{R}\left[\hat{K}_1(\hat{K}_1 \cdot \mathbf{L}) - \hat{K}_2(\hat{K}_2 \cdot \mathbf{L})\right] \quad . \tag{15}$$

In topographical application of hologrammetry we desire to produce fringes which correspond to depth from the observer. For this condition, the fringe vector $\underline{\underline{K}}_f$ must be parallel to the observation direction $\hat{K}_2$. If translation is to be used to generate contour fringes on the object then, from Eq. 15 it is clear that $\underline{\underline{L}}$ must be perpendicular to $\hat{K}_1$. The fringes corresponding to this translation are generated along the lines of intersection of object's surface with equidistant fringe-locus planes which are normal to the direction of observation. The distance d between these planes is inversely proportional to the magnitude of $\underline{\underline{K}}_f$ and is defined as $d = \pi / |\underline{\underline{K}}_f|$. Thus, having computed d, we can accurately determine coordinates of any point on the surface of the object under investigation.

Surface roughness measurement

Recent studies of statistical properties of laser speckle patterns led to development of new methods for measurement of surface roughness. When compared with mechanical methods of surface roughness measurement, the speckle techniques are advantageous because they are noncontact, nondestructive, are relatively easy to handle, and have potential for mass-production industrial applications.

Depending on the rms roughness to be measured, three different speckle techniques can be distinguished. For measuring fine-scale surface roughness, less than 0.25 μm, the coherent light speckle contrast method is used [22]. For moderate surface roughness, 0.2 - 5 μm, polychromatic speckle pattern method applies [23]. Finally, for rough surfaces, 1 - 30 μm, technique based on speckle pattern correlation gives the best results [24]. Since speckle pattern correlation technique would have most extensive photogrammetric applications, it will be briefly discussed herein, for discussion of the other two methods References 4, 22, and 23 should be consulted.

In the speckle pattern correlation method, the rough surface under examination is illuminated by a coherent plane wave from a laser, Fig. 4a. The speckle pattern produced by a wave incident on the surface is recorded, in the Fraunhofer diffraction region, in a suitable photographic emulsion placed normal to the direction defined by an angle θ_2. Then, the angle of incidence is varied by a small amount $\delta\theta_1$ and a second exposure is made on the same emulsion. This change of the incidence angle from θ_1 to $\theta_1+\delta\theta_1$ produces a decrease in correlation between the two speckle patterns which is a function of the surface roughness. The degree of correlation is directly related to the visibility of Young's fringes (Fig. 4b), which are produced at the focal plane of a reconstructing lens (Fig. 4c), from the two speckle patterns recorded in the film. Visibility V of these fringes is related to the surface roughness R_S by

$$V = \tfrac{1}{2} \exp\left\{ -\tfrac{1}{2}\left[\left(\frac{2\pi}{\lambda}\right) \frac{\sin(\theta_1 + \theta_2)}{\cos\theta_2} R_s \delta\theta_1 \right]^2 \right\} . \qquad (16)$$

Equation 16 clearly indicates that surface roughness can be measured by determining the visibility of Young's fringes as a function of $\delta\theta_1$ when the geometric parameters θ_1 and θ_2 as well as the wavelength λ are fixed.

Other representative applications of hologrammetry

Hologrammetry is finding ever increasing application in vibration analysis, because of the simplicity of the method. We merely need to vibrate the object while making a hologram of it, develop the hologram, and observe the reconstruction. Fringes that are seen in the reconstruction connect all points of common amplitude and are represented by a zero-order Bessel function of the first kind, whose argument is realated to the vibration amplitude of the object. Extensive theory of holographic vibration analysis has been developed by Stetson [25].

A recent development and use of an image derotator has made it possible to extend the techniques of hologram interferometry and speckle metrology to the vibration analysis of rotating objects [26]. The combination of holography and speckle metrology, together with the variation in pulse separation, allows for a very wide range of vibration amplitudes to be recorded. The technique applies to contoured objects, to resonant and nonresonant vibrations, and to speeds up to 10 000 rpm. Because of the importance of

vibration analysis of rotating structures, the image derotator system is of considerable engineering value.

Hologrammetry is widely used in nondestructive testing of various components including microcrack detection (Fig. 5), inspection of laminated structures and composite materials, pressure vessel inspection, etc. These and other applications are carried out with computer compatible video systems. Such systems enable data to be acquired optically and processed electronically, thus providing very versatile instruments.

Although it may seem, from the foregoing dicussion, that hologrammetry and related techniques are only useful in research and industrial applications, they are, nontheless, ideally suited for certain studies in biostereometrics. In particular, hologrammetry allowed accurate, non-invasive quantification of cranio-facial and dental displacements in three-dimensional space [27-29].

References

1. R. J. Pryputniewicz, Laser Holography, Worcester Polytechnic Institute, Worcester, MA (1979).

2. R. J. Pryputniewicz and K. A. Stetson, Fundamentals and Applications of Laser Speckle and Hologram Interferometry, Worcester Polytechnic Institute, Worcester, MA (1980).

3. R. K. Erf, ed., Holographic Nondestructive Testing, Academic Press, New York (1974).

4. R. K. Erf, ed., Speckle Metrology, Academic Press, New York (1978).

5. K. A. Stetson, "A review of speckle photography and interferometry," Opt. Engrg., 14:482 (1975).

6. C. M. Vest, Holographic Interferometry, Wiley, New York (1979).

7. J. W. C. Gates, "Photogrammetry and optical metrology," Proc. ISP Comm. V, Stockholm (1978).

8. W. Schumann and M. Dubas, Holographic Interferometry, Springer Verlag, Berlin (1979).

9. K. A. Stetson, "The use of projection matrices in hologram interferometry," in press: J. Opt. Soc. Am.

10. R. J. Pryputniewicz, "The properties of fringes in hologram interferometry," Proc. 1st Internat. Symp. on Hologram Interferometry and Speckle Metrology, Cape Cod, MA (1980).

11. R. J. Pryputniewicz and W. W. Bowley, "Techniques of holographic displacement measurement: an experimental comparison," Appl. Opt., 17: 1748 (1978).

12. R. J. Pryputniewicz and W. W. Bowley, "Holographic analysis of airfoils," Proc. ISP Comm. V, Stockholm (1978).

13. R. J. Pryputniewicz, "Use of projection matrices in specklegraphic

displacement analysis," Proc. SPIE (1980).

14. R. Dändliker, B. Ineichen, and F. M. Mottier, "High resolution hologram interferometry by electronic phase measurement," Opt. Commun., 9:412 (1973).

15. M. Dubas and W. Schumann, "The determination of strain in holographic interferometry using the line of complete localizations," Optica Acta, 22:807 (1975).

16. K. A. Stetson, "Homogenous deformations: determination by fringe vectors in hologram interferometry," Appl. Opt., 14:2256 (1975).

17. R. J. Pryputniewicz and K. A. Stetson, "Holographic strain analysis: extension of fringe vector method to include perspective," Appl. Opt., 15:725 (1976).

18. R. J. Pryputniewicz, "Holographic strain analysis: an experimental implementation of the fringe vector theory," Appl. Opt., 17:3613 (1978).

19. R. J. Pryputniewicz, "Determination of the sensitivity vectors directly from holograms," J. Opt. Soc. Am., 67:1351 (1977).

20. R. J. Pryputniewicz and K. A. Stetson, "Determination of sensitivity vectors in hologram interferometry from two known rotations of the object," in press: Appl. Opt.

21. K. A. Stetson, "The relationship between strain and derivatives of observed displacement in coherent optical metrology," in press: J. Opt. Soc. Am.

22. H. Fujii, T. Asakura, and Y. Shindo, "Measurement of surface roughness properties by using image speckle contrast," J. Opt. Soc. Am., 66:1217 (1976).

23. H. M. Penderson, "On the contrast of polychromatic speckle patterns and its dependence on surface roughness," Optica Acta, 22:15 (1975).

24. D. Léger, E. Mathieu, and J. C. Perrin, "Optical surface roughness determination using speckle correlation technique," Appl. Opt., 14: 872 (1975).

25. K. A. Stetson, "Holographic vibration analysis," in Holographic Nondestructive Testing, R. K. Erf, ed., Academic Press, New York (1974).

26. K. A. Stetson, "The use of an image derotator in hologram interferometry and speckle photography of rotating objects," Exp. Mech., 18:67 (1978).

27. R. J. Pryputniewicz, "Holographic determination of rigid-body motions and application of the method to orthodontics," Appl. Opt., 18:1442 (1979).

28. R. J. Pryputniewicz and C. J. Burstone, "The effect of time and force magnitude on orthodontic tooth movement," J. Dent. Res., 58:1754 (1979).

29. R. J. Pryputniewicz and C. J. Burstone, "Application of hologram interferometry in studies of cranio-facial and dental displacements," in press: J. Biomech.

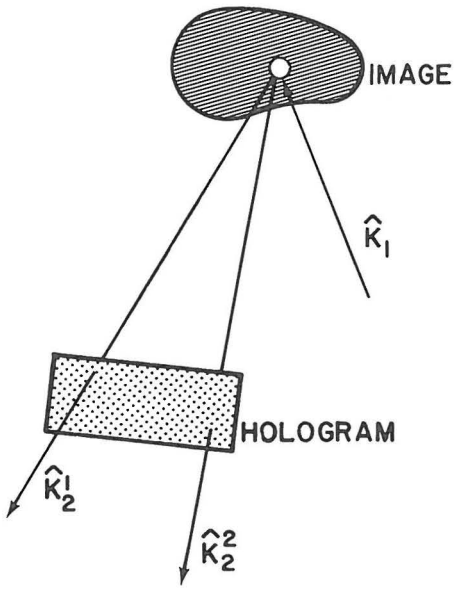

Fig. 1. Multiple observations of an image through a single hologram.

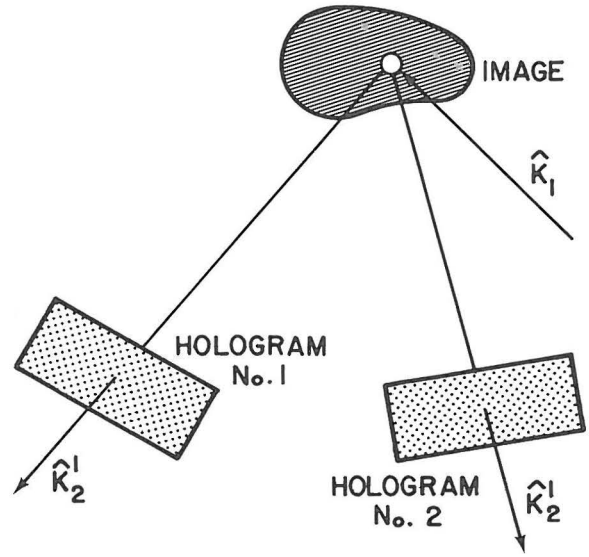

Fig. 2. Use of multiple holograms in analysis of a single image.

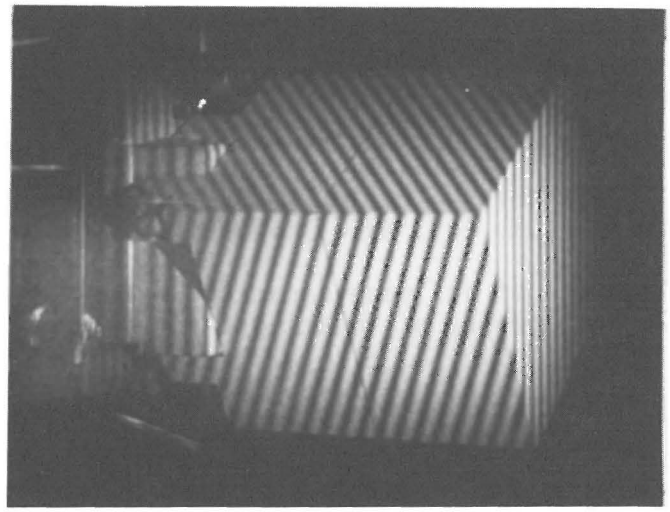

Fig. 3. Photograph of a typical reconstruction from a double-exposure hologram recording rotation of an object.

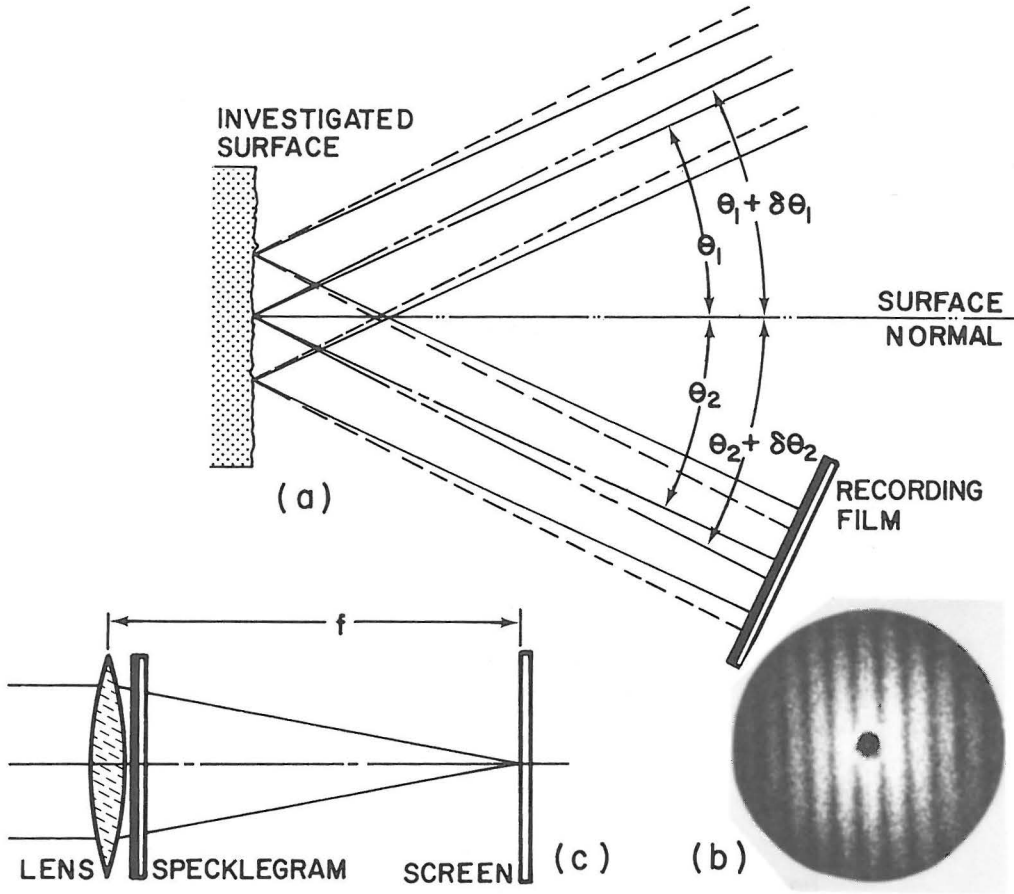

Fig. 4. Surface roughness measurement by speckle pattern correlation method: (a) recording geometry, (b) Young's fringes at the Fourier transform plane obtained using the arrangement shown in (c).

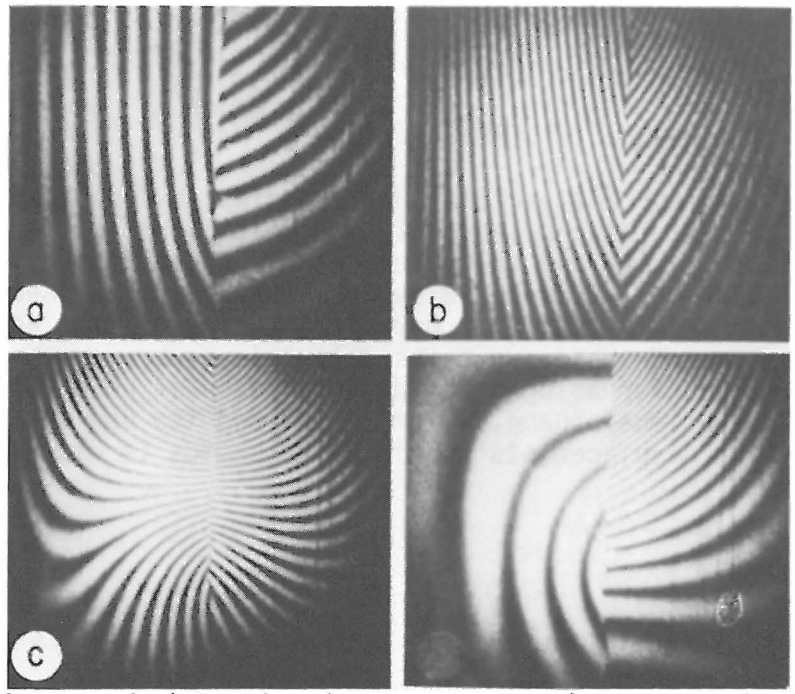

Fig. 5. Microcrack detection in porous ceramic components. In (a) to (d) the test component remains the same, only the point of force application is changed. Discontinuity in a fringe pattern clearly indicates presence of a crack.